Geochemical constraints on the tectonic setting of the Sonakhan Greenstone Belt, Bastar Craton, Central India

S. D. Deshmukh, K. R. Hari, P. Diwan & M. P. Manu Prasanth

Acta Geochimica

ISSN 2096-0956

Acta Geochim
DOI 10.1007/s11631-017-0213-z

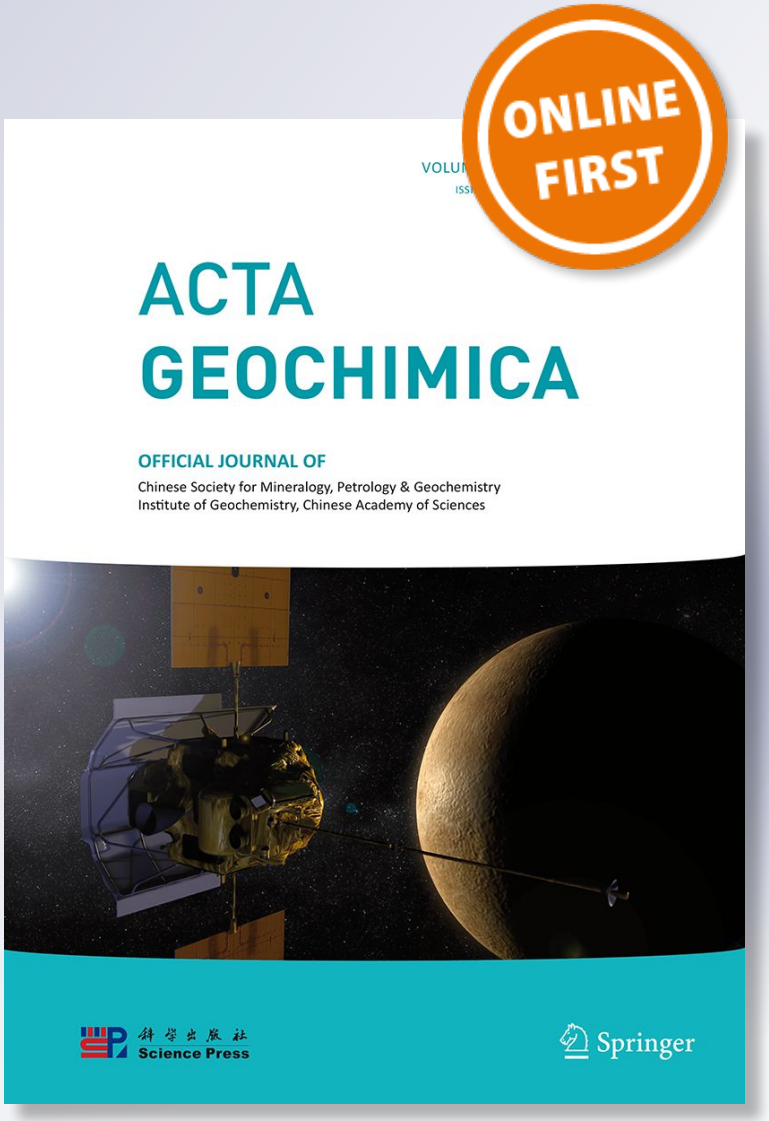

Springer

Acta Geochim
DOI 10.1007/s11631-017-0213-z

ORIGINAL ARTICLE

Geochemical constraints on the tectonic setting of the Sonakhan Greenstone Belt, Bastar Craton, Central India

S. D. Deshmukh[1] · K. R. Hari[2] · P. Diwan[3] · M. P. Manu Prasanth[2]

Received: 19 August 2016 / Revised: 30 March 2017 / Accepted: 16 August 2017

Abstract The Neo-Archean Sonakhan Greenstone Belt (SGB) located in the north-eastern fringes of Bastar craton, Central India, is dominated by Basalts, Andesites, Dacites and Rhyolites association. Partial melting modeling on the SGB metabasalts indicates that these rocks were derived by 20% melting of spinel peridotite. Fractional crystallisation modeling with REE reveal that the most evolved samples represent the product of fractional crystallization of least evolved magma with 35% plagioclase, 35% clinopyroxene, 20% olivine, 5% magnetite and 5% ilmenite as fractionating minerals with 40% remaining magma. Depletion of HFSE with reference to the LILE and LREE/HFSE ratios and Nb, Zr anomalies in the multi-element diagram of the mafic rocks of SGB indicate Island arc magmatic setting. The enriched Th/Yb values further substantiate that the mantle arrays were modified by subduction-related fluids or melts. The general conclusions drawn indicate that the metabasalts from the SGB were formed as a result of subduction of an intraoceanic lithosphere in a fore-arc suprasubduction zone environment.

Keywords Supra-subduction · Neo-Archean · Sonakhan Greenstone terrain · Bastar craton

✉ K. R. Hari
krharigeology@gmail.com

[1] Department of Geology, Govt. V. Y. T. P G Autonomous College, Durg, Chhattisgarh, India

[2] School of Studies in Geology and W.R.M., Pt. Ravishankar Shukla University, Raipur, Chhattisgarh, India

[3] Department of Applied Geology, National Institute of Technology, Raipur, India

1 Introduction

The nature of petrogenetic and geodynamic process behind the generation of Archean continental crust still remains one of the most challenging problems in Earth Science (Hawkesworth et al. 2010; Foley et al. 2002; Rapp et al. 2003; Xiao and Santosh 2014; Zhai 2014). Occurrence of Greenstone-Gneiss association is a common feature of Archean cratons (Naqvi 2005). The term Greenstone Belt is generally used to describe elongated to variably-shaped terrain of variable length and width, consisting of spatially and temporally related materials from (1) Archean to Proterozoic intrusive and extrusive ultramafic, (2) mafic to felsic rocks commonly associated with variable amounts and types of metasedimentary rocks, and (3) intruded by granitoid plutons. 85% of the ophiolite occurrences in the greenstone sequences can be classified as the subduction-related tectonic environment. Subduction unrelated greenstone occurrences are mainly developed during ocean basin evolution, and are related to continental rifting, seafloor spreading drift-rift tectonics and plume magmatism (Furnes et al. 2014, 2015).

The Peninsular Indian Shield, which is made up of low to high-grade metamorphic terrain, has an age range of 3.6–2.6 Ga. These terrain attained tectonic stability for prolonged periods, and they constitute continental crust designated as cratons (Naqvi and Rogers 1987; Balasubramanyan 2006; Ramakrishnan and Vaidyanadhan 2008). Stabilization of a craton occurs when intruded by plutons, and as a result, the whole-rock isotopic systems become closed so platform sedimentation takes place on the newly formed basement (Rogers and Santosh 2003). The Bastar Craton, which is located in the eastern part of Peninsular India, is bordered by the Satpura mobile belt in the north, the Pranhita–Godavari rift in the south, the Deccan Traps

Published online: 29 August 2017

in the west, the Eastern ghats mobile belt in the east and the Mahanadi rift in the north east (Ramchandra et al. 2001; Ramakrishnan and Vaidyanadhan 2008).

The prominent Greenstone Belts of Peninsular India can be classified into the Keewatin-type and the Dharwar type (Radhakrishna 1976). The Keewatin-type (which includes Hutti-Maski, Sandur, Ramgiri and Kolar belts) can be comparable with other Archaean Greenstone Belts of the world; the Dharwar-type (which includes Bababudan, Chitradurga–Gadag, and Dharwar–Shimoga belts), on the other hand, are akin to the Proterozoic belts of a basinal and geosynclinal type (Radhakrishna and Ramakrishnan 1988, 1990). The Sonakhan Greenstone Belt (SGB), located in the Northeastern part of Bastar Craton belongs to the Keewatin type. SGB covers an area of about 1200 km^2 and represents a late Archaean volcano-sedimentary sequence with mafic and felsic metavolcanic rocks along with Banded Iron Formation, comprised of sedimentary sequences of conglomerate, greywacke, argillite and ferruginous chert (Arjuni Formation) (Deshmukh et al. 2006, 2008; Ramchandra et al. 2001; Yedekar et al. 1990; 2003). In the present work, major and trace element geochemical characteristics of metabasalts from SGB are evaluated to elucidate the tectonic setting of the terrain.

2 General geology of the Sonakhan Greenstone Belt

The SGB, with NW–SE trend, is almost perpendicular to the NE-SW trending Central Indian Tectonic Zone CITZ (Fig. 1). Based on the Rb–Sr data on meta rhyolites of SGB, Ghosh et al. (1995) proposed that the Sonkhan greenstone terrain formed around 2.5 Ga. However no detailed geochemical and isotopic studies are available from this terrain. The Baghmara Formation in the Sonakhan Greenstone terrane is a suite mainly composed of mafic metabasalts with subordinate rhyolite and tuffaceous materials. The mafic metavolcanic rocks of Baghmara Formation are represented by pillowed and massive/schistose metabasalts. Ray et al. (2000) and Ray and Rai (2004) reported potential gold mineralization from the SGB. Venkatesh (2001) carried out ore mineralogical studies in this terrane and proposed a mesothermal origin for gold mineralization. Deshmukh et al. (2008) reported komatiitic affinity for the metabasalts of the SGB and correlated SGB with the Hutti Greenstone Belt of the Dharwar Craton.

3 Petrography

The mineral assemblages exhibited in the metabasalts are as follows:

Plagioclase + actinolite + chlorite + opaques ± clinopyroxene ± epidote ± apatite

In metabasalt, the overall abundance of plagioclase phenocrysts ranges from 5% to 15%. The other phenocryst phases include clinopyroxene and amphibole (Fig. 2a). The groundmass consists of plagioclase, clinopyroxene, amphibole, magnetite and sporadic apatite. In some sections, flow texture is also perceptible (Fig. 2b). Secondary phases in some of the samples include chlorite, epidote, and calcite.

4 Geochemistry

The geochemical analysis was carried out in order to determine the major oxides concentration by X-Ray Fluorescence spectrometry (XRF) Philips-1400 (Holland) instrument. Rare earth elements (REE), high field strength elements (HFSE), large ion lithophile elements (LILE) and transition metals (Ni, Co, Cr, V, and Sc) were analyzed using the ICP-MS technique by ELAN DRC II (Perkin Elmer Sciex Instrument, USA) at the National Geophysical Research Institute, Hyderabad, India.

Deshmukh et al. (2008) reported the major element geochemistry of the mafic rocks of SGB and argued a komatiite affinity for these rocks. In the present paper, we are presenting the trace element data of the same samples presented in Deshmukh et al. (2008). For the convenience of the readers, we are incorporating major element data from Deshmukh et al. (2008) (Table 1) along with the new trace element data.

Traditionally, magmatic rocks are classified on the basis of the Total Alkali-Silica (TAS) diagram either by Le Bas et al. (1986) or by Le Bas and Streckeisen (1991). However, the metamorphism and hydrothermal reactions in the greenstone terrain increases the mobility of Na and K. Therefore, classification of igneous rocks in greenstone terrain on the basis of TAS diagram may not be appropriate. Hence, in order to give a proper nomenclature of the rocks, in the present work, we are using Zr/Ti–Nb/Y diagram (Floyd and Winchester 1975). When the samples were plotted in the Zr/Ti–Nb/Y diagram, it was found that all the plots fall in "basaltic field" (Fig. 3).

Chondrite-normalized REE pattern of all the rocks are similar (Fig. 4) and have a typical flat REE [$(La/Lu)_n = 1–1.5$] pattern, which is a characteristic feature of komatiite related rocks. Condie (1989) proposed that the flat REE pattern is a characteristic feature of Archean Greenstone Belts with a komatiitic affinity (TH-1type). Incompatible trace element abundances (Table 1) in comparison to the Primitive mantle suggests that most of the SGB metabasalts are characterised by selective enrichment

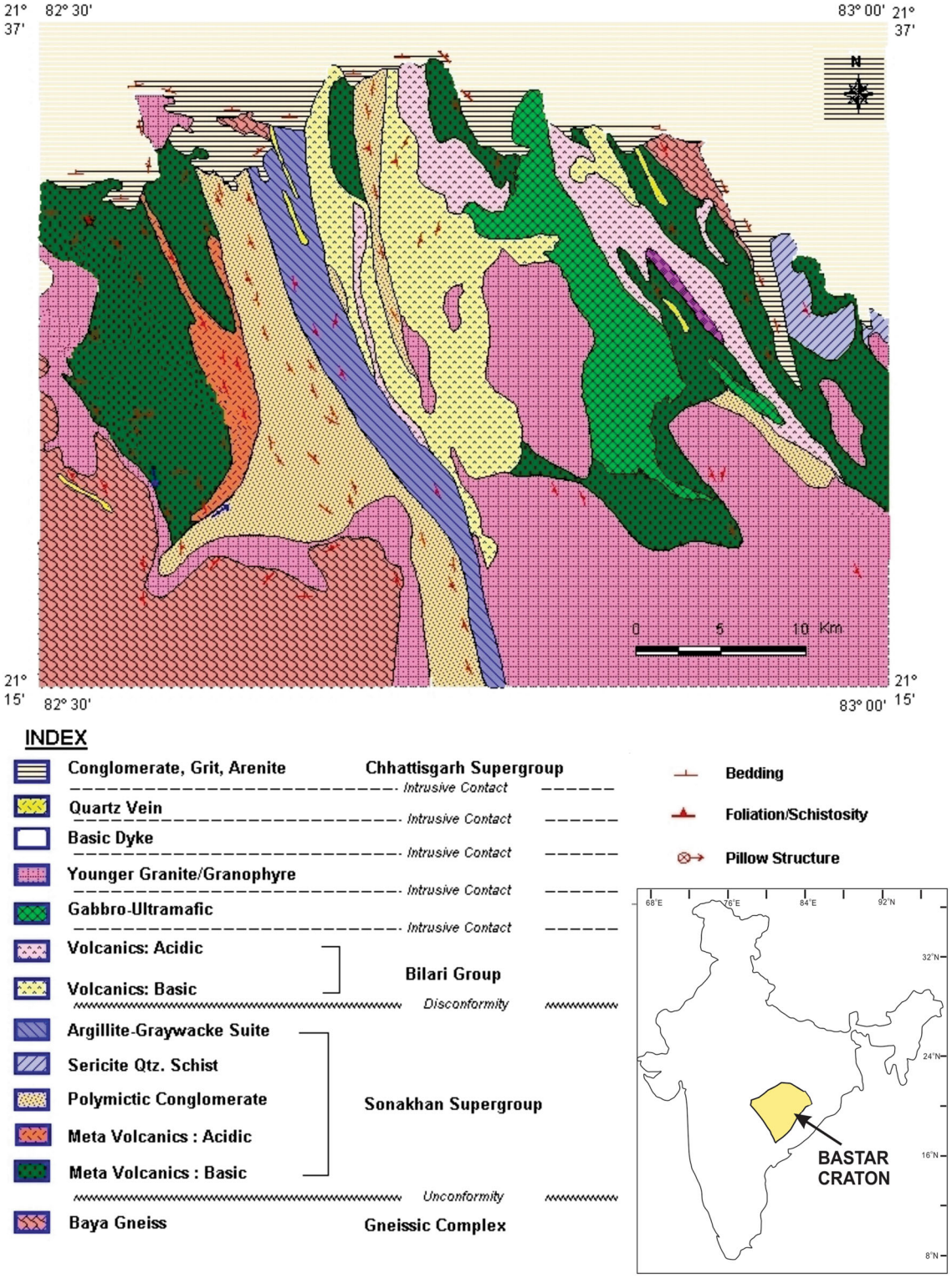

Fig. 1 Regional geological map of Sonakhan Greenstone Terrane (after Das et al. 1990)

of Large Ion Lithophile Elements (LILE), such as Rb, Ba, and Sr, and relative depletion of High Field Strength Elements (HFSE) such as Nb, P, Ti, Y, and Yb. The primitive mantle normalized multi-element spider diagram is characterized by pronounced negative Nb and Zr anomalies (Fig. 5). The presence of negative Nb anomaly indicates a subduction-related genesis (Pearce 1982). Positive anomalies of Pb and Ta were also observed. Sajona et al.

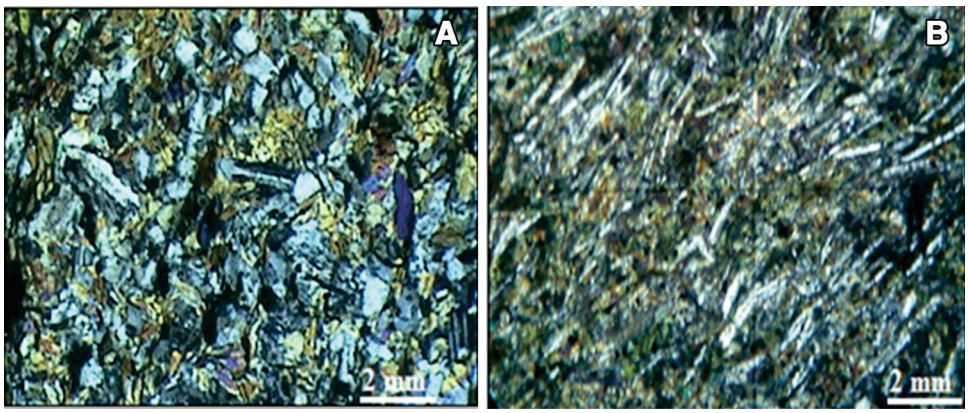

Fig. 2 Photomicrographs of meta basalts of Sonakhan Greenstone Belt

(1996) proposed that the island arc basalts have low Nb content (<2 ppm). The low Nb content in the SGB meta-basalts (0.236–2.092 ppm) further substantiates subduction magmatism.

5 Discussions

5.1 Elemental mobility

Elemental mobility during post-magmatic alteration and metamorphism is a point of concern in the Archaean volcanic rocks (Polat et al. 2002). It has been concluded by various workers (Ludden et al. 1982; Rajamani et al. 1985; Xie et al. 1993; Arndt 1994; Kröner et al. 2013; Polat 2013) that the effects of alteration on HFSE, Ti, Cr, Ni, and REE (except Eu) are relatively insignificant (Pearce and Peate 1995). The element Zr is often used as an alteration index of metamorphosed volcanic rocks (Pearce 2014; Rollinson 1999). The mobility of LILE such as Rb, K, Sr and Ba is well documented in Archaean volcanic rocks (Arndt and Goldstein 1989; Arndt 1994).

A general consensus exists that field, petrographic and geochemical criteria may be applied for the evaluation of alteration sensitivity (mobility or immobility of elements) in volcanic rocks that have experienced submarine hydrothermal alteration and metamorphism. These criteria include the preservation of primary volcanic features such as pillows, uniform inter-element ratios and smooth REE patterns (excepting Ce and Eu) etc. However, submarine alteration and metamorphism might have affected the geochemistry of original volcanic rocks to a variable extent as seen in the thin sections. Therefore, the mobility of elements has to be evaluated prior to their application in petrogenetic modeling.

During hydrothermal processes, some major elements such as Ti, Al, and P are generally immobile, whereas others like Na and Ca are almost always mobile (MacGeehan and MacLean 1980; Mottl 1983). At greenschist facies metamorphic conditions, Si, Ti, Al, Mn, and P remain unchanged, whereas Fe, Mg, Na, and K may be mobilized (Pearce 1982; Rollinson 1993). Usefulness of major element data is therefore often conditional on unknown factors of metamorphism. Therefore, in the present case, in order to evaluate the effect of metamorphism and hydrothermal alteration, we have to focus on the behavior of the trace elements. The mobility of trace elements in metamorphism can be generalized into two groups. (1) Low field strength (LFS) elements (Cs, Sr, K, Rb, and Ba) are generally mobilized, whereas (2) high field strength (HFS) elements (REE, Sc, Y, Th, Zr, Hf, Ti, Nb, Ta, and P) are relatively immobile (Pearce, 1982). Further, Co, Ni, V, and Cr are also considered immobile (Rollinson 1993). The linear trends are shown with Zr and Hf, because when plotted against Y, they indicate their immobile nature and thus can be used for petrogenetic modeling (Fig. 6a, b).

5.2 Magma generation and modification

The tholeiite sequences with komatiitic affinity in the Archaean Greenstone Belts (TH-1 of Condie 1989) generally exhibit a flat REE pattern. Condie and Harrison (1976) studied the Maric Formation in the Midlands Greenstone Belt of Rhodesia and carried out petrogenetic modeling of TH-1, proposing that it is produced by 30% partial melting of a lherzolite source with olivine, clinopyroxene, orthopyroxene and spinel as residual minerals. Arth and Hanson (1975) proposed that TH-1 tholeiite from northwestern Minnesota was derived by 10–25% partial melting of the mantle. The REE patterns of meta-basalts of Baghmara Formation closely resemble those of TH-1 from Minnesota, thus pointing towards a similar mantle-melting pattern. When SGB samples were plotted in the La/Yb versus Dy/Yb diagram, they fall in the stability field of spinel peridotite (Fig. 7). Modeling of the samples of SGB was carried out using non-modal batch melting process (Baker et al. 1997) with La/Yb ratio. The modeling was carried out considering the sample with

Table 1 Major and trace element concentrations of mafic metavolcanics of Sonakhan Greenstone Belt (major element values are from Deshmukh et al. 2008)

Sample	SK-1	SK-2	SK-5	SK-5/7	SK-6	SK-8	SK-9	SK-10	SK-15
SiO_2	53.31	54.81	49.18	53.22	51.34	53.26	53.9	51.27	53.55
TiO_2	0.81	0.64	0.96	0.72	0.92	0.78	0.75	0.78	0.65
Al_2O_3	13.32	13.32	12.61	11.64	14.66	12.96	15	12.39	15.87
Fe_2O_3	12.86	11.23	12.31	12.76	14.08	11.37	10.66	12.43	10.85
MnO	0.16	0.17	0.19	0.17	0.18	0.17	0.17	0.17	0.16
MgO	8.42	7.93	4.31	6.86	5.61	6.32	6.05	7.25	6.81
CaO	9.06	10.07	11.64	10.44	11.4	11.26	10.78	10.48	9.62
Na_2O	0.93	0.65	1.69	1.77	0.51	2.81	1.31	2.69	0.77
K_2O	0.12	0.46	0.67	0.32	0.14	0.13	0.16	0.68	0.38
P_2O_5	0.09	0.08	0.09	0.07	0.1	0.07	0.09	0.08	0.09
Total	99.08	99.36	93.65	97.97	98.94	99.13	98.87	98.22	98.75
Sc	39.473	36.277	43.514	39.825	24.615	40.503	24.905	41.105	42.584
V	269.34	241.87	283.2	251.05	157.27	267.77	159.85	263.05	256.23
Cr	103.74	180.35	137.05	204.09	188.135	235.31	89.821	228.44	222.8
Co	168.212	161.965	159.16	152.9	257.89	514.2	263.54	170.963	150.025
Ni	57.854	85.77	71.67	73.884	60.33	102.1	61.338	80.792	73.753
Cu	114.62	113.78	44.409	103.77	474.25	540.57	481.76	76.351	154.57
Zn	112.41	131.25	108.02	97.859	69.666	103.09	70.741	95.77	96.008
Ga	12.342	12.582	15.614	12.592	7.606	12.292	7.737	12.516	12.964
Rb	13.427	24.051	19.478	8.461	12.3	13.302	2.293	13.819	9.656
Sr	125.42	105.93	165.16	94.271	66.969	152.29	66.845	136.55	100.21
Y	22.244	16.083	22.056	19.031	15.753	19.368	15.917	18.579	19.667
Zr	44.686	21.437	22.578	15.479	17.848	12.736	17.664	13.862	14.983
Nb	1.692	1.519	2.092	1.511	1.027	0.236	1.01	1.493	1.578
Cs	0.864	3.334	1.637	0.326	0.944	0.112	0.948	0.529	0.475
Ba	27.197	106.26	175.97	62.165	23.081	56.91	23	56.236	82.64
La	3.375	3.426	4.158	3.883	1.81	2.578	1.83	2.415	3.643
Ce	8.445	8.523	9.679	8.972	4.884	6.722	4.888	6.592	8.624
Pr	1.05	0.982	1.157	1.046	0.633	0.869	0.63	0.864	1.072
Nd	6.562	5.882	7.315	6.362	4.175	5.653	4.229	5.688	6.552
Sm	1.867	1.648	2.16	1.748	1.241	1.747	1.292	1.631	1.797
Eu	0.711	0.644	0.961	0.666	0.528	0.665	0.524	0.572	0.695
Gd	2.942	2.449	3.094	2.643	1.994	2.593	1.966	2.421	2.651
Tb	0.55	0.427	0.58	0.481	0.373	0.496	0.373	0.45	0.484
Dy	3.172	2.424	3.281	2.755	2.267	2.812	2.286	2.658	2.846
Ho	0.686	0.522	0.702	0.606	0.51	0.623	0.512	0.579	0.62
Er	2.285	1.628	2.225	1.934	1.616	2.051	1.645	1.993	2.026
Tm	0.391	0.283	0.388	0.347	0.27	0.342	0.269	0.334	0.343
Yb	2.113	1.495	1.933	1.84	1.347	1.864	1.382	1.783	1.925
Lu	0.324	0.215	0.294	0.294	0.205	0.284	0.199	0.274	0.31
Hf	1.187	0.612	0.725	0.61	0	0	0	0.489	0.64
Ta	0.451	0.363	1.502	0.433	0.514	0.224	0.486	0.35	0.408
Pb	2.726	5.65	8.021	6.951	9.773	7.562	9.091	4.158	7.468
Th	0.586	0.961	0.474	0.753	0.191	0.33	0.172	0.329	0.674
U	0.112	0.139	0.117	0.212	0.044	0.084	0.042	0.083	0.111

lowest REE values (SK-6), and the results revealed these rocks were generated by ~20% partial melting of a spinel lherzolite (Fig. 8).

Various differentiation processes have to be evaluated in detail for finding out the reason for magma modification. In the present case, fractional crystallization, which is the

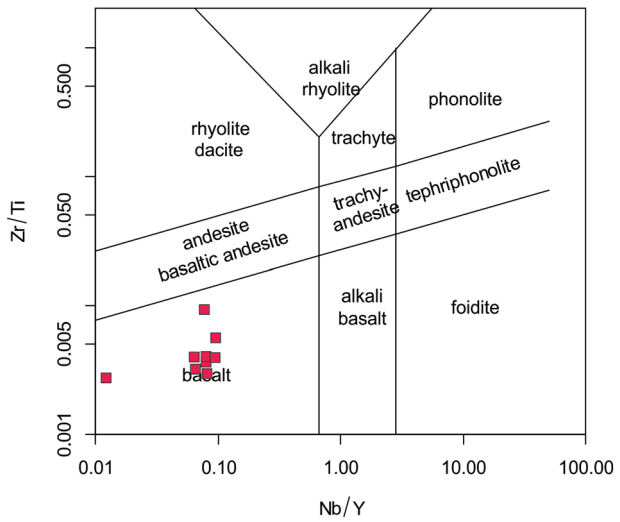

Fig. 3 Zr/Ti versus Nb/Y diagram of mafic meta volcanics from the Sonakhan Greenstone Belt (Pearce 2008)

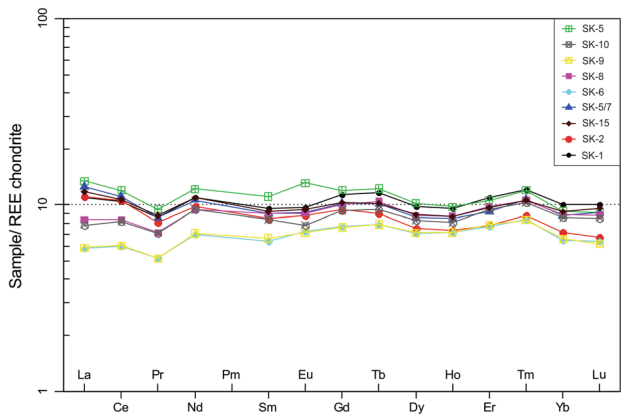

Fig. 4 Chondrite normalized REE diagram of meta basalts from the Sonakhan Greenstone Belt (Normalizing factors are from Boynton 1984)

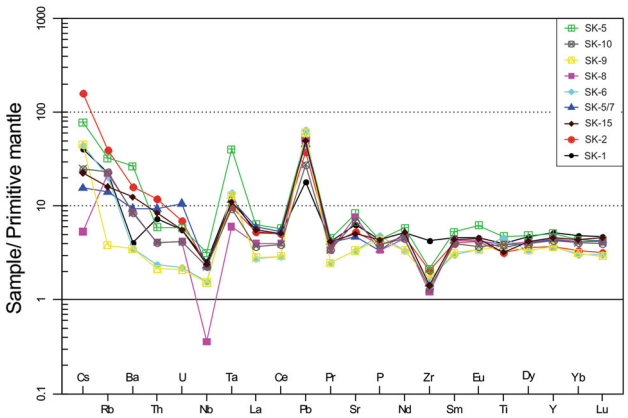

Fig. 5 Primitive mantle normalized multi element diagram of meta basalts from the Sonakhan Greenstone Belt (Normalizing factors are from McDonough and Sun 1995)

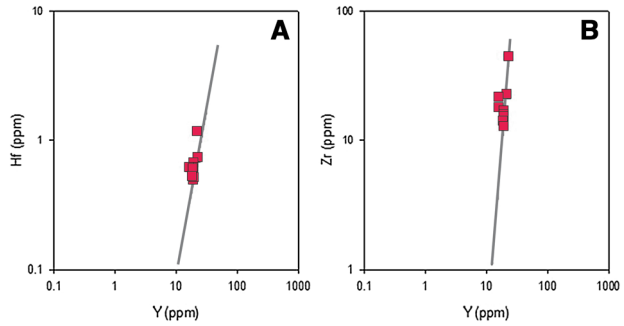

Fig. 6 **a** Hf versus Y and **b** Zr versus Y diagrams indicating a linear geochemical trend for the meta basalts of SGB

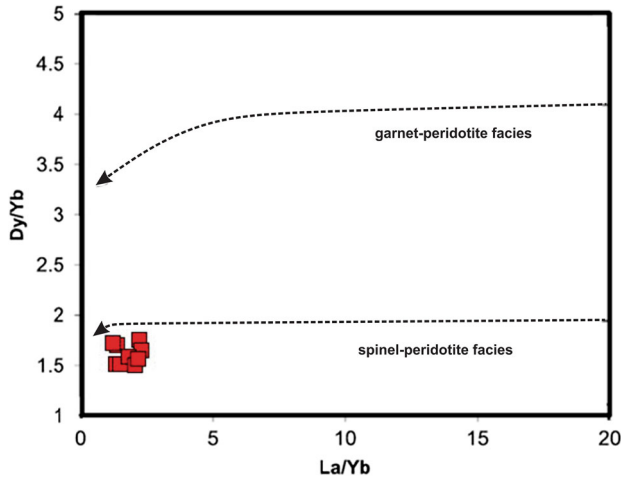

Fig. 7 Dy/Yb versus La/Yb plot for the meta basalts from SGB indicating their generation at shallower depths in spinel-peridotite stability field (Jung et al. 2006)

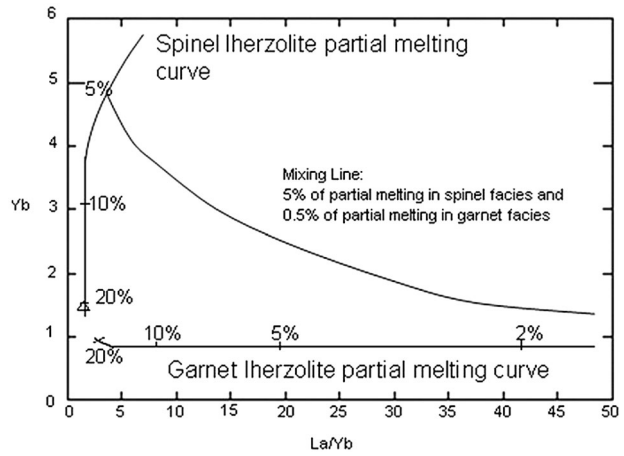

Fig. 8 La/Yb versus Yb diagram showing model melting curves for non-model fractional melting of garnet and spinel lherzolite facies (Baker et al. 1997). Numbers on the curves represent the percentage of melting of model mantle

most important magma modification process, has been evaluated with the help of trace elements. In the La/Sm-La diagram, data points plot along a nearly horizontal line (Fig. 9), indicating that fractional crystallization (Allegre and Minster 1978) has played a vital role in the modification of magma. The positive relationship between Ni and Mg# (Fig. 10a) indicates fractional crystallization of olivine minerals (Wilson 1989). Sc is compatible in pyroxene but not in olivine (Rollinson 1993), and the positive correlation of Sc with Mg# indicate pyroxene fractionation (Fig. 10b).

To evaluate the role of fractional crystallization, Rayleigh's fractional crystallization model was used. The sample SK-6 exhibits the minimum values for REE ($\Sigma_{REE} = 21.85$ ppm), and it was considered as representative of the least fractionated magma in the whole assemblage. In contrast, the sample SK-51 with highest REE ($\Sigma_{REE} = 51.92$ ppm) was considered as the final product of fractional crystallization. It is evident from the variation diagrams and chondrite normalized diagrams that olivine, clinopyroxene, and plagioclase were the governing phases in the fractional crystallization. As these rocks are of tholeiite nature, it can be assumed that olivine governed the crystal fractionation to a lesser degree than clinopyroxene and plagioclase. For fractional crystallization modeling, the fractionating minerals considered were plagioclase, clinopyroxene olivine, magnetite, and ilmenite. Modeling with REE revealed that the most evolved samples represented the product of fractional crystallization of SK-6 with 35% plagioclase, 35% clinopyroxene, 20% olivine, 5% magnetite and 5% ilmenite as fractionating minerals with 40% residual liquid (Fig. 11).

5.3 Geodynamic setting of SGB

During subduction, Ti becomes depleted in the source, whereas V is enriched in the source magma. As the oxidation increases due to subduction-derived fluids,

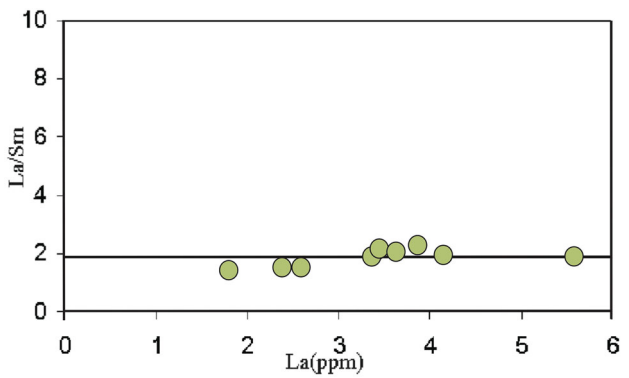

Fig. 9 La/Sm versus La Plots of SGB in a nearly horizontal line, indicating importance of fractional crystallization

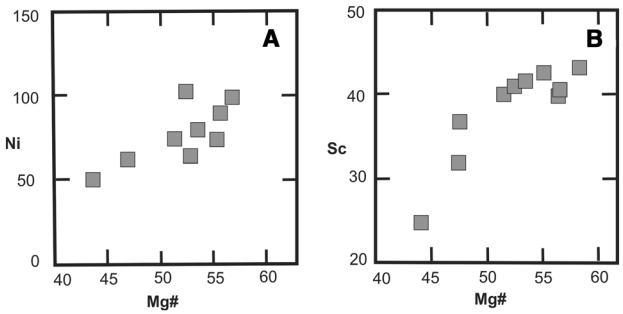

Fig. 10 Mg# values of SGB samples plotted against **a** Ni and **b** Sc

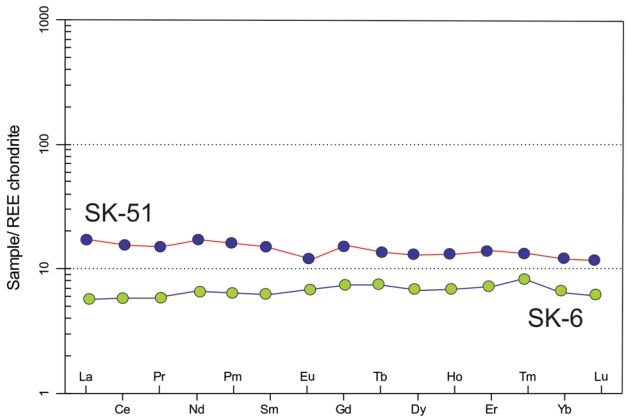

Fig. 11 REE modeling results for fractional crystallization

vanadium becomes more incompatible than in the lower oxidation state. Thus, higher Ti/V ratio indicates a subduction influenced source region (Shervais 1982). From Ti-V diagram (Fig. 12) it was observed that all samples except two were characterized by island arc setting. Scattering of

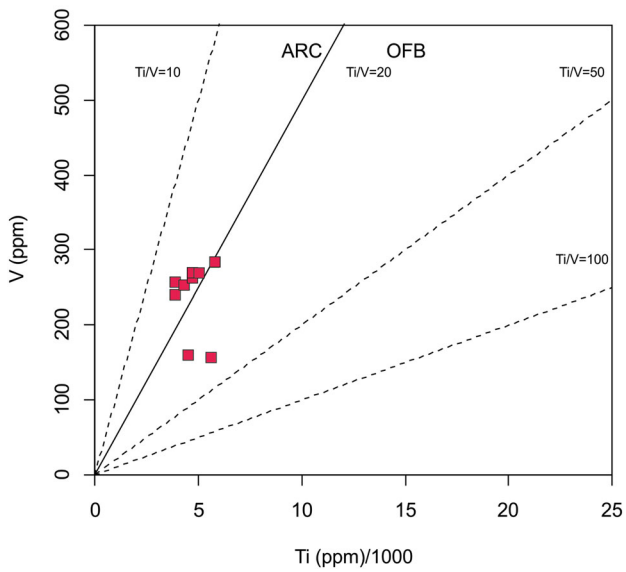

Fig. 12 V versus Ti tectonic discrimination diagram (Shervais 1982) of mafic metavolcanics of Sonakhan Greenstone Belt

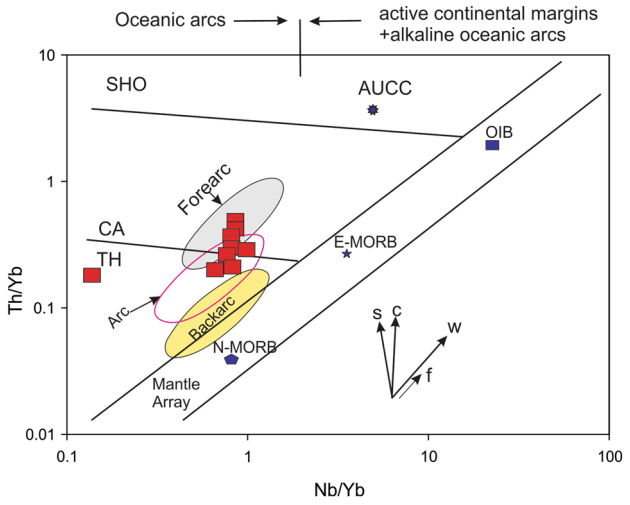

Fig. 13 Plot of Th/Yb versus Nb/Yb for meta basaltic rocks of SGB. The mantle array includes constructive plate boundary magmas (*N-MORB* normal mid-ocean ridge basalts, *E-MORB* enriched mid ocean ridge basalts) and within-plate alkaline basalts (*OIB* ocean island basalts). AUCC is Archean upper continental crust. Fields for convergent margin basalts include the tholeiitic (TH), calc-alkaline (CA), and shoshonitic (SHO) magma series. The vectors S, C, W, and f refer to subduction zone component, crustal contamination, within plate fractionation, and fractional crystallization respectively (after Pearce 2008). Forearc, arc, and backarc fields are of recent convergent margins fields are from Metcalf and Shervais (2008)

the samples may be due to the varied metasomatic effect or other post-magmatic alterations.

The classification scheme proposed by Pearce (2008) was followed in the next step. According to Pearce (2008), if the mantle arrays were modified by subduction-derived fluids, it would be enriched in Th. As a result, the Th/Yb ratio would be higher in subduction-related components than that of the mantle array. The basaltic rocks in the present area, when plotted in the Th/Yb versus Nb/Yb diagram (Fig. 13), fall in the volcanic arc array with arc-fore arc signatures. For further confirmation on the subduction-related genesis of SGB, we carried out the geochemical screening method proposed by Condie (1989). The average values of basaltic rocks from the terrane were compared with four screens, and it was found that the rocks were characterized by subduction-related genesis (Table 2). The elemental ratios of Nb/La (0.455467), Ti/Y (252.3778), in first order of SCREEN 1 and Ti/V (20.56667), TiO_2 (0.778889), Ta (0.525667) and Nb (1.350889) values in the second order of SCREEN 1 clearly exhibited the arc basalt tectonic setting for the SGB. Hf/Th (0.953691) and Ce/Nb (5.53783) ratios indicated N-MORB in SCREEN 2. From SCREEN 3 the values of Th/Yb (0.283615), Th/Nb (0.45622), Nb/La (0.455467) exhibited arc basalt characteristics. In SCREEN 4, Zr/Y

Table 2 Geochemical screening of meta basalts of SGB (after Condie 1989)

Screen 1	WPB-MORB	ARC-N MORB	Pillow lavas of Baghmara Formation
First order			
Nb/La	>1	≤1	0.455467
Ti/Y	≥350	<350	252.3778
Second order			
Ti/V	>30	≤30	20.56667
TiO_2	>1.25	≤1.25	0.778889
Ta	>.7	≤0.7	0.525667
Nb	>12	≤12	1.350889
Screen 2	WPB T-EMORB	N MORB	
Hf/Th	<8	≥8	0.953691
Ce/Nb	≤2	>2	5.53783
Screen 3	NMORB	ARCB	
Th/Yb	≤0.1	>0.1	0.283615
Th/Nb	≤0.07	>0.07	0.45622
Nb/La	>0.8	≤0.8	0.455467
Screen 4	IAB-CABI	CABC	
Zr/Y	<3	≥3	0.924893
Ta/Yb	≤0.1	>0.1	0.030336
Screen 5	IAB	CABI	
Th/Yb	≤0.3	>0.3	0.283615
Ti/Zr	≥85	<85	322.0413

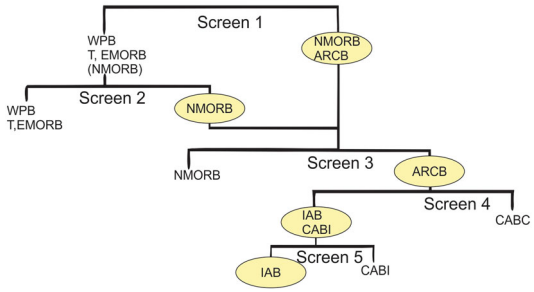

Fig. 14 Flow chart depicting tectonic classification of mafic metavolcanics from Sonakhan Greenstone Belt (Condie 1989)

(0.924893) and Ta/Yb (0.030336) exhibited IAB-CABI character. IAB tectonic framework of the metabasalts from SGB was confirmed with Th/Yb (0.283615) and Ti/Zr (322.0413) ratios from SCREEN 5. Figure 14 depicts a flow chart illustrating different screening methods marked with the behavior of SGB metabasalts on each screen. The chemical composition of subduction zone magmas generated in the convergent boundaries was mainly controlled by two sources: the mantle wedge and the slab components (i.e., fluids and/or melts generated from the subducting slab) (Tatsumi et al. 1986; Morris et al. 1990; Hawkesworth et al. 1993; Pearce and Peate 1995; Pearce 2008).

Deshmukh et al. (2017) proposed a subduction-related genesis for the felsic metavolcanic rocks of Bagmara formation of SGB. Prominent negative Nb anomaly in the multi-element spider diagram, along with other elemental fingerprints, clearly indicated subduction magmatism (Keleman et al. 2004; Pearce, 2008; Perfit et al. 1980; Tatsumi et al. 1986; Pearce and Stern 2006; Hawkesworth et al. 1993; Pearce and Peate 1995). In an arc-related environment, the subducted slab underwent dehydration during the initial stage of subduction. The subducting slab dehydrated, and the subduction-derived fluids caused the metasomatism of the mantle wedge. However, the differences in the melting process in a subduction-related environment were primarily due to the difference in P_{H2O} (Manning 2004; Mibe et al. 2011; Anderson et al. 1980) The higher P_{H2O} in an arc-related environment incorporated LILE and LREE into the melt phase and as a result, the residual mantle became enriched in HFSE. Depletion of HFSE with reference to the LILE and LREE/HFSE ratios and Nb, Zr anomalies, which were perceptible in the mafic rocks of SGB, were characteristic features of Island arc magmas (Fig. 5) (Pearce 2008; Manning 2004; Wilson and Davidson 1984). The enrichment in LILE indicated that the SGB metabasalts were derived as a result of metasomatism of the depleted mantle wedge beneath the Bastar Craton. The Archean geothermal gradient, size and dynamics of plates collectively played a significant role in the generation of these basaltic rocks. Various studies at Archean greenstone terrane imply that the Neoarchean convergent margins, wedge melting, arc magmatism and slab dehydration were the prominent mechanisms involved in the generation of arc basaltic magma (Wyman 2003; Kerrich et al. 1998, Wyman and Kerrich 2009; Lafleche et al. 1992).

Acknowledgements SDD expresses his sincere thanks to Dr. S. K. Rajput, Principal, Govt. V.Y.T.PG Autonomous College, Durg. The authors are also thankful to Dr. Sandeep Vansutre and Dr. Shailesh Agrawal for their help in the preparation of the manuscript. Financial support from UGC to S.D. Deshmukh is gratefully acknowledged.

References

Allegre CJ, Minster JF (1978) Quantitative models of trace element behavior in magmatic processes. Earth Planet Sci Lett 38(1):1–25

Anderson RN, Stephen ED, Schwarz WM (1980) Dehydration, asthenospheric convection and seismicity in subduction zones. J Geol 88:445–451

Arndt NT (1994) Archean komatiites. Dev Precambrian Geol 11:11–44

Arndt NT, Goldstein SL (1989) An open boundary between lower continental crust and mantle: its role in crust formation and crustal recycling. Tectonophysics 161(3):201–212

Arth JG, Hanson GN (1975) Geochemistry and origin of the early Precambrian crust of northeastern Minnesota. Geochim Cosmochim Acta 39(3):325–362

Baker JA, Menzies MA, Thirlwall MF, MacPherso CG (1997) Petrogenesis of Quaternary intraplate volcanism, Sana'a, Yemen: implications for plume–lithosphere interaction and polybaric melt hybridization. J Petrol 38(10):1359–1390

Balasubramanyan MN (2006) Geology and tectonics of India: an overview. International Association of Gondwana Research, Kochi, Japan, p 206

Boynton WV (1984) Cosmochemistry of the rare earth elements; meteorite studies. In: Henderson P (ed) Rare earth element geochemistry. Elsevier Sci. Publ. Co., Amsterdam, pp 63–114

Condie KC (1989) Geochemical changes in basalts and andesites across the Archean Proterozoic boundary: identification and significance. Lithos 23:1–18

Condie KC, Harrison NM (1976) Geochemistry of the archean Bulawayan group, Midlands Greenstone Belt, Rhodesia. Precambrian Res 3(3):253–271

Das N, Royburman K, Vatsa US, Mahurkar VY (1990) Sonakhan Schist Belt, a Precambrian granite—greenstone complex. Geol Surv India Spec Publ 28:118–132

Deshmukh SD, Hari KR, Diwan P (2006) Pillow Lavas of Baghmara Formation (Sonakhan Greenstone Belt), Central India: geochemical constraints from major elements. Gond Geol Mag 21(1):37–42

Deshmukh SD, Hari KR, Diwan P, Basavarajappa HT (2008) Spinifex textured metabasalt from Sonakhan Greenstone Belt, Central India. Indian Miner 42:71–83

Deshmukh SD, Hari KR, Diwan P, Manu Prasanth MP (2017) Geochemistry and petrogenesis of felsic meta-volcanic rocks of Baghmara Formation, Sonakhan Greenstone Belt, Central India. J Geosci Res 2(1):69–74

Floyd PA, Winchester JA (1975) Magma type and tectonic setting discrimination using immobile elements. Earth Planet Sci Lett 27:211–218

Foley S, Tiepolo M, Vannucci R (2002) Growth and early continental crust controlled by melting of amphibolite in subduction zones. Nature 417:837–840

Furnes H, De Wit M, Dilek Y (2014) Four billion years of ophiolites reveal secular trends in oceanic crust formation. Geosci Front 5(4):571–603

Furnes H, Dilek Y, De Wit M (2015) Precambrian greenstone sequences represent different ophiolite types. Gondwana Res 27(2):649–685

Ghosh S, Rajajaiya V, Ashiya ID (1995) Rb-Sr dating of components from the Sonakhan Granite-Greenstonebelt, Raipur District. MP Rec Geolo Surv India 128:11–13

Hawkesworth CJ, Gallagher K, Hergt JM (1993) Mantle and slab contributions in arc magmas. Annu Rev Earth Planet Sci 21:175–204

Hawkesworth CJ, Dhuime B, Pietranik AB, Cawood PA, Kemp AI, Storey CD (2010) The generation and evolution of the continental crust. J Geol Soc 167:229–248

Jung C, Jung S, Hoffer E, Berndt J (2006) Petrogenesis of Tertiary mafic alkaline magmas in the Hocheifel, Germany. J Petrol 47(8):1637–1671

Keleman PB, Hanghoj K, Greene AR (2004) One view of the geochemistry of subduction-related magmatic arcs with an emphasis on primitive andesite and lower crust. In: Holland HD, Turekian KK (eds) Treatise on geochemistry 3. Elsevier, Amsterdam, pp 593–659

Kerrich R, Wyman DA, Fan J, Bleeker W (1998) Boninite series: low Ti-tholeiite associations from the 2.7 Ga Abitibi Greenstone Belt. Earth Planet Sci Lett 164:303–316

Kröner A, Hoffmann JE, Xie H, Wu F, Münker C, Hegner E, Wong J, Wan Y, Liu D (2013) Generation of early Archaean felsic greenstone volcanic rocks through crustal melting in the Kaapvaal craton, southern Africa. Earth Planet Sci Lett 381:188–197

Lafleche MR, Dupuy C, Dostal J (1992) Tholeiitic volcanic rocks of the late Archaean Blake River group, southern Abitibi Greenstone Belt: origin and geodynamic implications. Can J Earth Sci 29:1448–1458

Le Bas MJ, Streckeisen AL (1991) The IUGS systematics of igneous rocks. J Geol Soc Lond 148:825–833

Le Bas MJ, Lemaitre RW, Streckeisen A, Zanettin B (1986) A chemical classification of volcanic-rocks based on the total alkali silica diagram. J Petrol 27(3):745–750

Ludden J, Gélinas L, Trudel P (1982) Archean metavolcanics from the Rouyn-Noranda district, Abitibi Greenstone Belt, Quebec. 2. Mobility of trace elements and petrogenetic constraints. Can J Earth Sci 19(12):2276–2287

MacGeehan PJ, MacLean WH (1980) An Archaean sub-seafloor geothermal system, calc-alkali'trends, and massive sulphide genesis. Nature 286:767–771

Manning CE (2004) The chemistry of subduction-zone fluids. Earth Planet Sci Lett 223:1–16

McDonough WF, Sun SS (1995) Composition of the earth. Chem Geol 120:223–253. doi:10.1016/0009-2541(94)00140-4

Metcalf RV, Shervais JW (2008) Suprasubduction-zone ophiolites: Is there really an ophiolite conundrum? Geol Soc Am Spec Pap 438:191–222

Mibe K, Kawamoto T, Matsugake KN, Fei Y, Ono S (2011) Slab melting versus slab dehydration in subduction-zone magmatism. PNAS. doi:10.1073/pnas.1010968108/-/DCSupplemental

Morris JD, Leeman WP, Tera F (1990) The subducted component in island arc lavas: constraints from Be isotopes and B-Be systematics. Nature 344:31–36

Mottl MJ (1983) Metabasalts, axial hot springs, and the structure of hydrothermal systems at mid-ocean ridges. Geol Soc Am Bull 94(2):161–180

Naqvi SM (2005) Geology and evolution of the Indian plate. Capital Publishing, New Delhi, p 450

Naqvi SM, Rogers JJW (1987) Precambrian geology of India. Oxford University Press, Oxford, p 223

Pearce JA (1982) Trace element characteristics of lavas from destructive plate boundaries. In: Thorpe RS (ed) Andesites. Wiley, Chidester, pp 525–548

Pearce JA (2008) Geochemical fingerprinting of oceanic basalts with applications to ophiolite classification and the search for Archean oceanic crust. Lithos 100:14–48

Pearce JA (2014) Immobile element fingerprinting of ophiolites. Elements 10(2):101–108

Pearce JA, Peate DW (1995) Tectonic implications of the composition of volcanic arc magmas. Annu Revi Earth Planet Sci 23:251–285

Pearce JA, Stern RJ (2006) Origin of back-arc basin magmas: trace element and isotope perspectives. Back-arc spreading systems: geological, biological, chemical and physical interactions. Geophys Monogr Ser 166:66–86

Perfit MR, Gust DA, Bence AE, Arculus RJ, Taylor SR (1980) Chemical characteristics of island-arc basalts: implications for mantle sources. Chem Geol 30(3):227–256

Polat A (2013) Geochemical variations in Archean volcanic rocks, southwestern Greenland: traces of diverse tectonic settings in the early Earth. Geology 41(3):379–380

Polat A, Hofmann AW, Rosing Minik Thorleif (2002) Boninite-like volcanic rocks in the 3.7–3.8 Ga Isua Greenstone Belt, West Greenland: geochemical evidence for intra-oceanic subduction zone processes in the early Earth. Chem Geol 184(3):231–254

Radhakrishna BP (1976) Two greenstone groups in Dharwar Craton. Ind Miner 16:12–15

Radhakrishna BP, Ramakrishnan M (1988) Archaean-Proterozoic boundary in India. J Geol Soc Ind 32:263–278

Radhakrishna BP, Ramakrishnan M (eds) (1990) Archaean Greenstone Belts of South India. Geological Society of India, Mem. 19:497

Rajamani V, Shivkumar K, Hanson GN, Shirey AS (1985) Geochemistry and petrogenesis of amphibolites, Kolar Schist Belt, South India: evidence for komatiitic magma derived by low percentages of melting of the mantle. J Petrol 26(1):92–123

Ramakrishnan M, Vaidyanadhan R (2008) Geology of India, vol 1. Geological Society of India, p 994

Ramchandra HM, Roy A, Mishra VP, Dutta NK (2001) A critical review of the tectonothermal evolution of the Bastar Craton. MS Krishnan Cent Comm Nat Sem Geol Surv Ind Spec Publ 55:161–180

Rapp R, Shimizu N, Norman MD (2003) Growth of early continental crust by partial melting of eclogite. Nature 425:605–609

Ray RK, Rai KL (2004) Geological setting and petrogenesis of the auriferous metavolcanic complex of Sonakhan, Raipur district, Chhattisgarh. SAAEG J Ecol Geol 1:45–60

Ray RK, Pandey HK, Rai KL (2000) Geochemistry of Mafic volcanics associated with sulphide mineralization in Sonakhan, Raipur district, Madhya Pradesh. In: Gyani KC, Kataria P (eds) Proc nat Sem on 'Tectonomagmatism, Geochemistry and Metamorphism of Precambrian terrain.' Univ Dept of Geology Udaipur, pp 381–393

Rogers JJW, Santosh M (2003) Supercontinents in earth history. Gondwana Res 6:357–368

Rollinson HR (1993) A terrane interpretation of the Archaean Limpopo Belt. Geol Mag 130(06):755–765

Rollinson H (1999) Petrology and geochemistry of metamorphosed komatiites and basalts from the Sula Mountains Greenstone Belt, Sierra Leone. Contrib Miner Petrol 134(1):86–101

Sajona FG, Maury RC, Bellon H, Cotten J, Defant M (1996) High field strength element enrichment of Pliocene—Pleistocene Island Arc Basalts, Zamboanga Peninsula, Western Mindanao (Philippines). J Petrol 37(3):693–726

Shervais JW (1982) Ti–V plots and the petrogenesis of modern and ophiolitic lavas. Earth Planet Sci Lett 32:114–120

Tatsumi Y, Hamilton DL, Nesbitt RW (1986) Chemical characteristics of fluid phase from the subducted lithosphere: evidence from high-pressure experiments and natural rocks. J Volcanol Geother Res 29:293–309

Venkatesh AS (2001) Geochemical signatures and auriferous implications in Sonakhan Greenstone Belt, Chhattisgarh. Geol Surv India Spec Publ 55:219–228

Wilson M (1989) Igneous petrogenesis: a global tectonic approach. Unwyn Hyman, London

Wilson M, Davidson JP (1984) The relative roles of crust and upper mantle in the generation of oceanic island-arc magmas. Philos Trans R Soc Lond A 310:661–674

Wyman DA (2003) Upper mantle processes beneath the 2.7 Ga Abitibi belt, Canada: a trace element perspective. Precambrian Res 127:143–165

Wyman DA, Kerrich R (2009) Plume and arc magmatism in the Abitibi subprovince: implications for the origin of Archean continental lithospheric mantle. Precambrian Res 168:4–22

Xiao WJ, Santosh M (2014) The western Central Asian Orogenic Belt: a window to accretionary orogenesis and continental growth. Gond Res 25:1429–1444. doi:10.1016/j.gr.2014.01.008

Xie Q, Kerrich R, Fan J (1993) HFSE/REE fractionations recorded in three komatiite-basalt sequences, Archean Abitibi Greenstone Belt: implications for multiple plume sources and depths. Geochim Cosmochim Acta 57(16):4111–4118

Yedekar DB, Jain SC, Nair KKK, Dutta KK (1990) Central Indian collision suture. Geol Surv Ind Spec Publ 29:1–43

Yedekar DB, Karmalkar N, Pawar NJ, Jain SC (2003) Tectonomagmatic evolution of central Indian terrain. Gond Geol Mag Spec 7:67–68

Zhai MG (2014) Multi-stage crustal growth and cratonization of the North China Craton. Geosci Front. doi:10.1016/j.gsf.2014.01.003